J Mater Sci (2009) 44:3356–3363
DOI 10.1007/s10853-009-3436-5

Characterization of mechanical properties of FeCrBSiMnNbY metallic glass coatings

J. B. Cheng · X. B. Liang · B. S. Xu · Y. X. Wu

Received: 13 December 2008 / Accepted: 23 March 2009 / Published online: 16 April 2009

Abstract This article investigates mechanical characteristics of Fe-based metallic glass coatings. A series of the coatings were fabricated by conventional wire-arc spray process. The microstructure of the coating was characterized by means of X-ray diffraction, scanning election microscopy equipped with energy dispersive X-ray analysis, transmission electron microscopy, and differential scanning calorimeter. The coating is very dense smooth, adhering well and with no cracking. The microstructure of the coating consists of amorphous phase and α(Fe,Cr) nanocrystalline phase. The nanocrystalline grains with a size of 30 to 60 nm are homogenously dispersed in the amorphous phase matrix. The crystallization temperature of the amorphous phase is about 545 °C. The mechanical properties, such as porosity, adhesive strength, microhardness, elastic modulus, and abrasive wear resistance, were analyzed in detail. The experimental results indicate that the coating has high microhardness (15.74 GPa), high elastic modulus (216.97 GPa), and low porosity (1.7%). The average adhesive strength value of the coating is 53.6 MPa. The relationship between abrasive wear behavior and structure of the coating is discussed. The relatively wear resistance of metallic glass coating is about 7 and 2.3 times higher than that of AISI 1045 steel and 3Cr13 martensite stainless steel coating, respectively. The main failure mechanism of metallic glass coating is brittle failure and fracture. The Fe-based metallic glass coating has excellent wear resistance.

J. B. Cheng · Y. X. Wu
Shanghai Key Laboratory of Materials Laser Processing and Modification, Shanghai Jiaotong University, Shanghai 200240, China

J. B. Cheng (✉) · X. B. Liang · B. S. Xu
National Key Laboratory for Remanufacturing, Academy of Armored Force Engineering, Academician Office No. 21 Dujiakan, Changxindian Fengtai District, Beijing 100072, China
e-mail: chengjiangbo@hotmail.com

Introduction

In the past decades, metallic glasses have been of great interest not only for fundamental studies, but also for potential applications [1, 2]. Since an Fe-based amorphous alloy was synthesized for the first time in an Fe-(Al,Ga)-metalloid system in 1995 [3], a variety of Fe-based amorphous alloy systems have been prepared [4, 5]. In industrial fields, however, the application of Fe-based bulk metallic glasses (BMGs) as engineering materials is restricted because of the limited thickness, low toughness at room temperature, and high costs. In order to widen the industrial applications, exploiting attainable amorphous alloys as coatings is preferred since the applications would not be limited by the thickness of BMGs. Several coating technologies have been used to deposit metallic glass coatings, including laser cladding [6], plasma spraying [7, 8], high velocity oxygen fuel spraying [9, 10], cold gas dynamic spraying [11], magnetron sputtering [12], and the electro-spark deposition process [13]. Compared with synthesis methods mentioned above, wire-arc spray is considered as a simple, low cost, efficient coating process with an ability to produce dense coatings with a wide rate of material deposition [14]. In wire-arc spraying, a spray is formed by the atomization of molten or semi-molten droplets by the impingement of fast moving and continuously flowing atomization gas upon melting tips of consumable and electrical conductive wires. The wires are connected individually as anode and the other one as

cathode and fed together to ignite an arc at the shortest distance between the electrical conductive parts in wire tips [14]. During spraying, an individual splat is estimated to cool at a rate of $\sim 10^5$ K s^{-1} [15], which is suitable for forming an amorphous phase. This low-cost manufacturing process could potentially solve many wear and corrosion problems by producing high-performance coatings.

Excessive wear is an important failure mode in many engineering applications. The interest in tribological performances of metallic glasses is because of their unique mechanical properties and potential applications. For example, amorphous alloys have been proposed as coatings in dry bearing in space [16]. The viscous flow of amorphous alloys has been exploited to manufacture mechanical devices such as ultra-fine gear [17]. The first study of wear of metallic glass appeared in 1979 by Boswell [18] who studied the abrasive wear of $Pd_{78}Cu_{5.5}Si_{16.5}$ using a pin-on-disk apparatus. And there have been over 60 documents on the subject. Fleury et al. [19] studied the tribological properties of Mg, Cu, Ni, and Ti-based BMGs. Prakash [20] investigated abrasive wear behavior of Fe, Co, and Ni-based metallic glasses. The sliding friction and wear behavior of various metallic glasses have been studied by Klinger [21] and other researchers [22, 23]. Recently, Greer and Rutherford [24] have reviewed the wear characteristics of mostly Fe and Al-based amorphous alloys and related materials. The investigations did just not only include metallic glasses, but also related materials such as partially or fully crystallized alloys obtained by annealing. And the geometry of these alloys is varied, ranging from bulk to coatings. But a limited number of studies have been conducted on mechanical properties and three-body abrasive wear of metallic glass coatings prepared by the conventional wire-arc spray process.

In this study, experimental results on mechanical properties, and particular abrasive wear resistance, of Fe-based metallic glass coatings are presented. For individual coated samples, the microstructure and surface morphology of the coating was characterized. The porosity and microhardness were examined. The coatings to substrate adhesive strength and nano-mechanical properties of the coating were analyzed. The formation mechanism of the amorphous and nanocrystalline phase is discussed in detail. Moreover, wear resistance of the coating was evaluated with a wet sand rubber wheel abrasion tester at ambient temperature. The effect of microstructure on wear resistance of the coating is also discussed.

Experimental procedures

Materials and coating production

AISI 1045 steel plates (30 mm × 60 mm × 10 mm) with hardness of about $Hv_{100} = 204$ were used for substrates. The microstructure of AISI 1045 steel consists of pearlite and αFe. Prior to coating, the substrate was degreased by acetone, dried in air, and then grit-blasted. A self-designed HAS-2 wire-arc gun system was employed for coatings preparation. A Fe-based cored wire (Fe–Cr–B–Si–Mn–Nb–Y) of 2 mm diameter consisting of conventional alloys powders, such as ferroboron and ferrosilicon, was used as feedstock. The feedstock contains specific atomic ratios of elements to maximize glass forming ability (GFA). The outer skin of the wire is 1Cr17 ferrite stainless steel. The cored wire is a proprietary, seven-element, glass forming alloys containing (wt%) chromium (<15), boron (<5), silicon (<2), niobium (<7), manganese (<3), yttrium (<5), with the balance iron. The wire-arc spray process parameters were as follows: spraying voltage 36 V, wire feed rate 2.7 m min^{-1}, compressed air pressure 700 kPa, the stand-off distance 200 mm.

Coating characterization

The microstructures of the coatings were observed by using a Philips Quant 200 scanning election microscopy (SEM) equipped with an energy dispersive X-ray analysis apparatus and transmission electron microscopy (TEM, H-8010). Coating phase structures were determined by means of X-ray diffraction (XRD) with Cu K_α ($\lambda = 1.54$ Å) radiation, step 0.02° on a D8-Advance apparatus. Image analysis was done to measure porosity. The SEM images with magnification of 1000 and with at least 20 view-fields from different positions and coating cross sections were used for the porosity measurement.

Differential scanning calorimeter (DSC) measurement of the coating was conducted at a rate of 10 K/min from room temperature to 1000 °C in N_2 atmosphere using a STA-449 DSC instrument (NETZSCH Instruments Co., Ltd., Germany). The coating was first removed from the substrate, lightly ground on abrasive paper, and then pounded by a mortar into powders (about 10 mg) for DSC measurement.

Mechanical properties characterization

The adhesive strength of the coatings was measured following the ASTM standard C-633-01 [25]. Following recommendations of the standard, mild steel cylindrical samples of 25 mm diameter were used as testing specimens. The cylindrical samples were degreased by acetone, dried in air, and then grit-blasted. The Fe-based cored wire was sprayed onto cylindrical samples to a thickness of about 0.38 mm. The coated surface of the cylindrical sample was glued to another identical grit-blasted cylinder using epoxy adhesive film (E-7 adhesives, Shanghai Research Institute of Synthetic Resins, China) that does not

penetrate the coating upon heating and thus does not affect the adhesion strength result. After curing at 100 °C for 4 h, the glued cylinders were mounted in a tensile test machine (WDW-200D universal testing machine, made in China) equipped with a self-aligning fixture and pulled apart until the coating failed. For each experiment, five specimens were used.

Vickers hardness measurements were made on polished sample surfaces with HVS-1000 Vickers hardness tester using a load of 100 g on each material. Indentation parameters were set as 15 s loading time and average thickness was derived from five measurements. All of the measured microVickers hardness values are mean of ten indentations. The nano-mechanical properties of the cross section of the coatings were performed with a NanoTest 600 nano-indenter (Berkovich indenter) from Micro Materials Limited, Wrexham, UK. Indentations were performed in load-control mode to loads as high as 20 mN using a load rate of 0.5 mN/s. The maximum load was held constant for 15 s and then was unloaded at the rates as same as the loading one.

The abrasive wear resistance of the coatings was evaluated with a rubber wheel abrasion tester. The specimens were ground with mesh 800 emery paper before wear testing. About 300–800 μm quartz sand width was used, and test load was set to 150 N cm^{-2} during wear testing. The speed of the rotating wheel was 240 rpm. The wear test time was 5 min. Before and after the testing, the specimens were cleaned in acetone and wear loss was measured using a precision electronic balance with an accuracy of 0.1 mg. The worn surfaces were characterized by SEM. The AISI 1045 steel substrate and 3Cr13 martensite stainless steel coating prepared by wire-arc spray process (chemical compositions of 0.3C–13Cr–0.6Si–0.6Mn–85.5Fe in wt%, $Hv_{100} = 477$) were selected as comparison materials.

Results and discussion

Microstructure characterization

Figure 1 shows the XRD pattern of the coating. It can be seen that a broad halo peak appears at $2\theta = 43.5°$, confirming that an amorphous phase present in the coating. The characteristic diffraction peaks of α-Fe,Cr are present for the coated sample. Any other oxidized material peaks are not detected, indicating low oxide content in the coating.

An SEM image of cross section through the coating is shown in Fig. 2. It can be seen that the coating is very dense, smooth, and without cracks (Fig. 2a). Some pores exist as indicated by the very dark regions in the coating. In some area, the coating appearance is quite smooth and looks more like a bulk material than a sprayed coating (Fig. 2b). Figure 2b is a magnification of the A area in Fig. 2a. During spraying, the deposition of successive molten droplets would release latent heat in solidification, and localized reheating could occur [26]. This can lead to thermal softening by raising the temperature of the particles to the values near the glass transition temperature of the amorphous alloy [27]. This facilitates plastic deformation and mechanical interlocking of splats. This would clean the surfaces of the particles and promote metallurgical bonding at the particle/particle surfaces [27]. Therefore the coating presents what appears to be a very high density. The average porosity of the coating is determined to be 1.7% by image analysis. The chemical composition of the coatings (Fig. 2b) by EDAX analysis was $Fe_{64.82}Cr_{9.23}B_{20.69}Si_{1.9}Mn_{1.01}Nb_{1.8}Y_{0.55}$ (at.%).

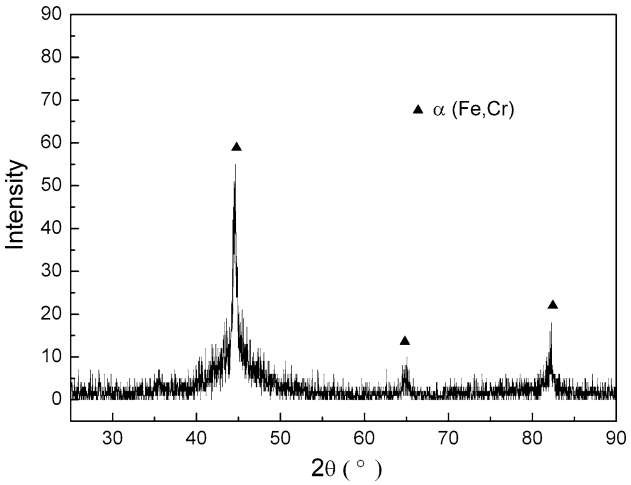

Fig. 1 XRD pattern of FeCrBSiMnNbY metallic glass coating

Figure 3 shows the surface morphology of the coating. Individual particles exhibit well-flattened splat and near disk-shape splat morphology with little splashing. This phenomenon indicates that the alloy system has excellent wetting behavior. The addition of B and Si acts to self-flux the alloy. Self-flux alloy primer indicates a nearly full density due to its relative low melting point and perfectly clean and bonded interface with the substrate and the topcoat [28]. And this means less porosity of the coating.

TEM was undertaken to obtain more details on microstructure formation, and is shown in Fig. 4. Figure 4a is a selected area electron diffraction (SAED) pattern of the coating. The diffused halo ring in the SAED pattern confirms that the coating is amorphous. The individual splat is estimated to cool at a rate of $\sim 10^5$ K s^{-1} during solidification [15], which is suitable for forming an amorphous phase. On the other hand, the Fe–Cr-B–Si–Mn–Nb–Y alloy system has very strong GFA, which satisfies the three

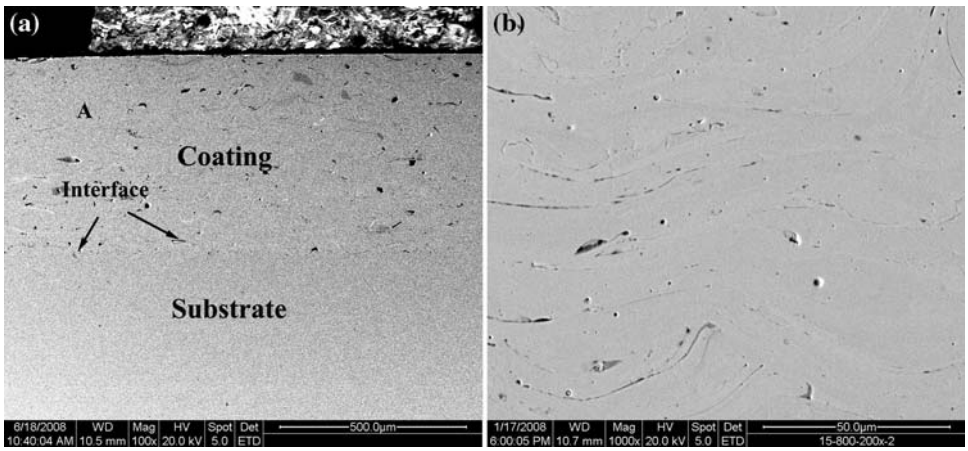

Fig. 2 SEM image of metal glass coating cross section: **a** low magnification, **b** high magnification

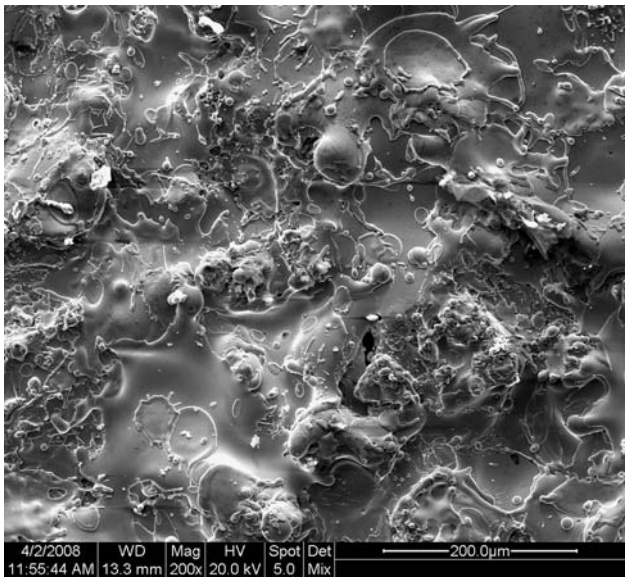

Fig. 3 SEM image of metal glass coating surface morphology

empirical rules proposed by Inoue et al. [29], i.e., (1) multicomponent alloy systems consisting of more than three constituent elements, (2) significantly different atomic size ratios above approximately 13%, and (3) suitable negative heats of mixing among the constituent elements. The atomic radius and mix enthalpy play important roles in glass formation [29]. The different atomic size in the order of Y > Nb > Cr > Mn > Fe > Si > B facilitate the packed local structure. The mixing enthalpies values for Fe–B, Fe–Si, Fe–Cr, Fe–Nb, and Fe–Y atomic pairs are −11, −18, −1, −16, and −1 kJ mol^{-1}, respectively. And the mixing-enthalpy values of the Cr–B, Cr–Nb, Nb−Si, B−Nb, Y−Mn, and Y−Si atomic pair are −16, −7, −31, −39, −8, and −57 kJ mol^{-1} [30]. Large negative heated mixing among the constituent elements strengthens the interaction among components and promotes the chemical short-range ordering in the liquid [31]. That means the formation of the amorphous phase is attributed to the high cooling rates of molten droplets and proper material composition.

However, the amorphous phase is a metastable phase, which can be transformed to a stable phase under suitable conditions. Figure 4b shows the microstructure of the coating with the nanocrystalline phase. The diffused halo ring in the SAED pattern confirms that the coating has an amorphous structure. The diffraction spots validate the

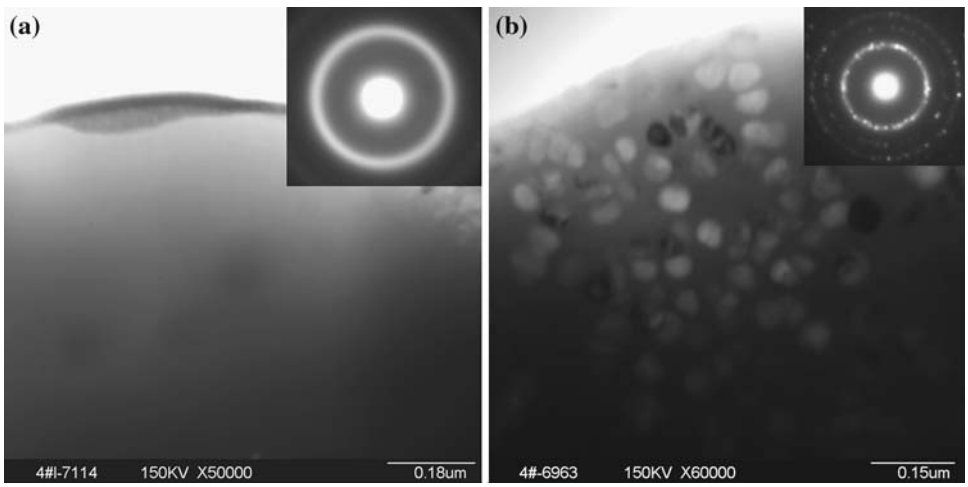

Fig. 4 TEM images of metal glass coating: **a** an amorphous phase region, **b** coexistence of nanocrystalline grains in an amorphous matrix. (*Inset*) SAD patterns are shown and exhibit diffuse rings (**a**) and spotty rings (**b**)

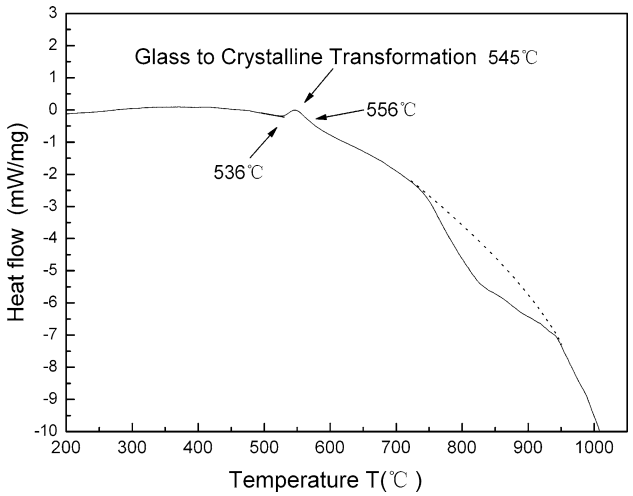

Fig. 5 DSC trace of FeCrBSiMnNbY metallic glass coating

existence of crystals in the coating. The microstructure of the coating consists of an amorphous phase matrix containing nanoparticles ranging in size from 30 to 60 nm.

DSC traces for the as-sprayed coating are shown in Fig. 5. An exothermic solid-state transformation is observed in the coating. From the figure, no glass transition temperature is been for in the coating, and the onset crystallization temperature T_x is 545 °C.

As mentioned above, the cooling rate of as-sprayed droplets is relatively high. This condition allows the formation of large numbers of small nuclei and fine nano-precipitates. The higher nucleation rate and fine nanostructures are highly dependent on the chemical composition, especially in the presence of glass forming elements [32]. The temperature in the arc can reach 5000 °C during spraying [33], which is much higher than onset crystallization temperature $T_x = 545$ °C. During the devitrification process, the glass precursor, when heated to its crystallization temperature, readily transforms into a nanocrystalline structure [34]. This refinement is due to the uniform nucleation and extremely high nucleation frequency during crystallization, resulting in little time for grain growth before impingement between neighboring grains. By this route, it is possible to develop very stable nanostructures that resist coarsening at elevated temperatures during spaying [35]. Figure 4 indicates that the coating is classified into two regions, namely, a full amorphous phase region and homogeneous dispersion of nanoscale particles in a residual amorphous matrix region.

Mechanical properties

Adhesive strength values for the coatings are in the range of 51 to 56 MPa. The average value is 53.6 MPa. This adhesive strength is remarkable for wire-arc coatings. The coating exhibits a high adhesive strength value because it has low porosity, excellent wettability, and adheres well to the substrate.

The microhardness profiles of the coatings across the thickness are shown in Fig. 6. The Vickers hardness is around $Hv_{100} = 900$–1000. Near the outside surface of the coating, the hardness increases slightly and exhibits a maximum value of $Hv_{100} = 1031$. This is thought to be affected by the thermal conditions affecting the amorphous phase including the droplet impingement temperature and cooling rate of the coating near the substrate [36].

The nano-mechanical properties of the coating and substrate are shown in Fig. 7. Typical Berkovich indentation image on cross section of the metallic glass coating is presented in Fig. 7. The nano-hardness and nano-elastic modulus of the coating can be calculated from the curve of load with displacement [37]. The nano-hardness of the

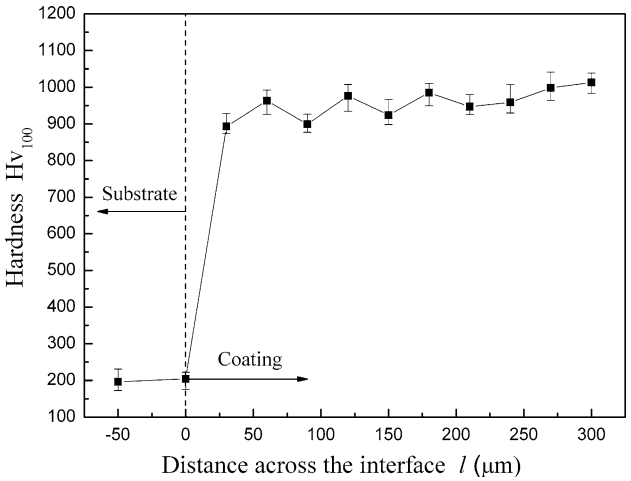

Fig. 6 Vickers hardness profile across the interface of metal glass coating

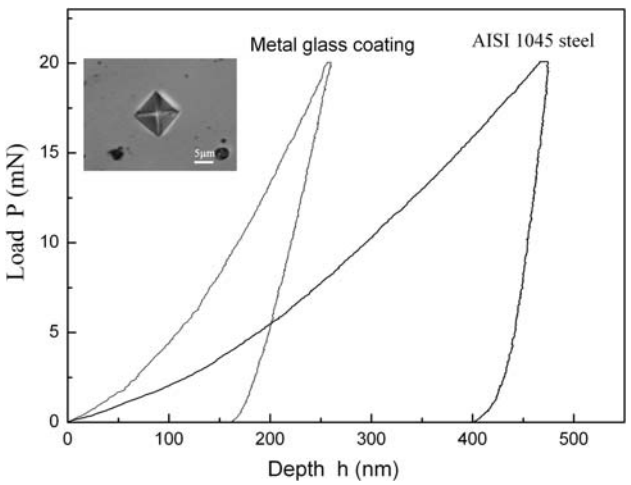

Fig. 7 Load–displacement curves of metal glass coating and AISI 1045 steel substrate

coating and that of AISI 1045 steel are 15.74 and 3.97 GPa, respectively. The nano-elastic modulus of the two materials is 216.97 and 209.43 GPa, respectively. The hardness/modulus of elasticity ratio (H/E ratio) for the coating is 0.06935, whereas that of the substrate is 0.01895. The elasticity of the amorphous/nanocrystalline coating is much higher than that of the substrate. The high H/E ratio has some beneficial influences on the wear resistance.

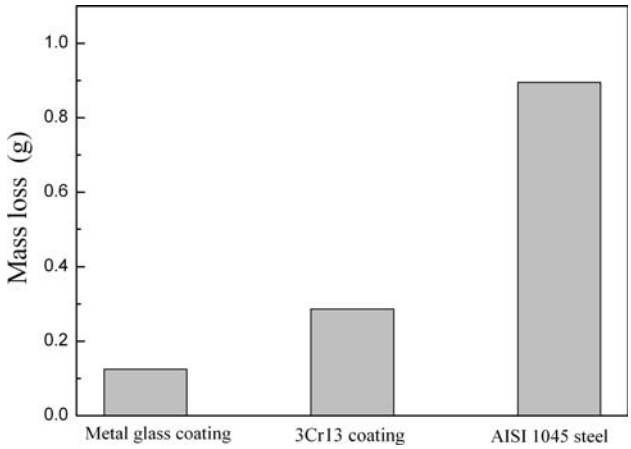

Fig. 8 Wear loss of coatings and substrate

Analysis of wear mechanisms

Figure 8 presents the wear loss of metallic glass coating, 3Cr13 martensite stainless steel coating, and substrate after wear testing. The mass loss of metallic glass coating is 0.1245 g and that of 3Cr13 coating and AISI 1045 steel are 0.2864 and 0.8952 g, respectively. Note that mass loss of metallic glass coating is the lowest among the testing materials, indicating that metallic glass coating has better resistance to abrasive wear. The relatively wear resistance of metallic glass coating is 7 and 2.3 times than that of substrate and 3Cr13 coating, respectively. The superior wear resistance of metallic glass coating can be explained by homogeneous dispersion of nanoscale particles into the glassy phase and prevent material removal.

The worn surface morphology is related to the wear mechanism. The worn surface of the substrate is distinguished by long continuous parallel grooves (see arrows in Fig. 9a), which formed as the hard abrasive particles dug into the sliding sample surface and then plowed out material to form a groove. This is an example of groove-wear mode. For this case, cutting and plowing are the main abrasive wear mechanisms. Figure 9b is the worn surface of 3Cr13 coating. The worn surface is relatively rough and

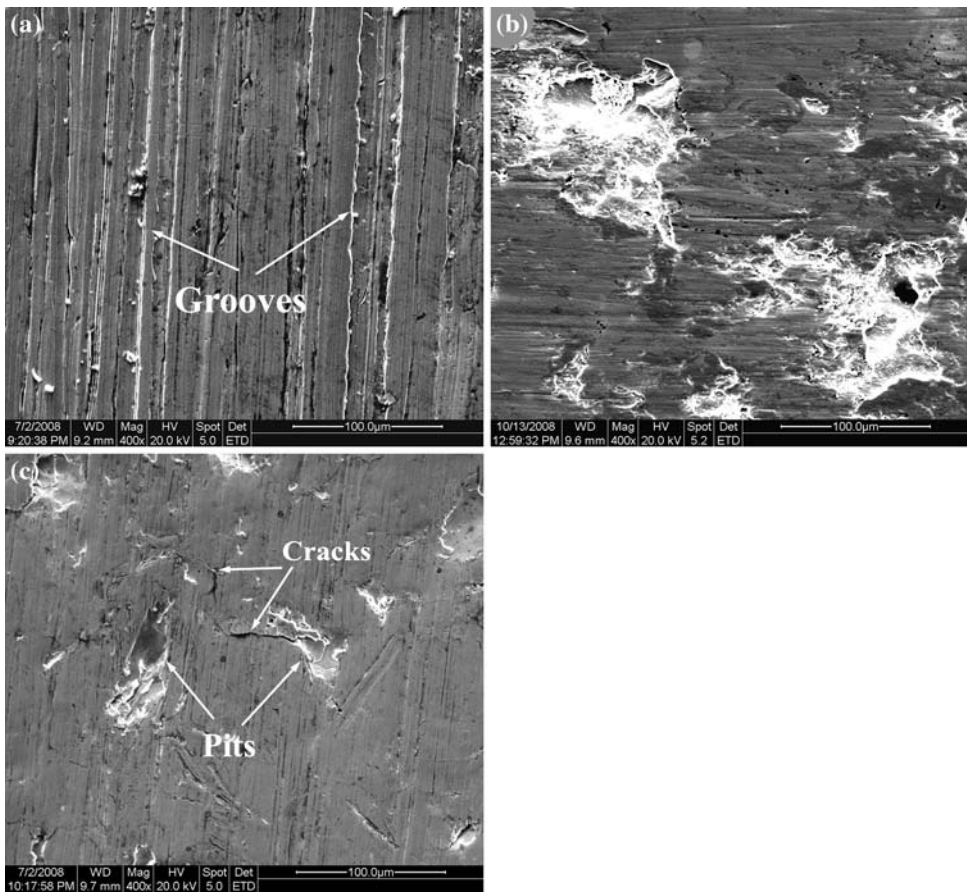

Fig. 9 SEM micrographs of the worn surface **a** substrate, **b** 3Cr13coating, and **c** metal glass coating

big pits exist in the coating, which means much materials loss. However, the worn surface of metallic glass coating with few cracks and small pits (Fig. 9c) is smoother than that of 3Cr13 coating. During the wear process, the abrasive particles dug into the sliding sample surface, and deformation of coating takes place inside of coating splats initially. Small craters and microcracks are formed by these moves. As the abrasive proceeds, propagation of the initial cracks occurs during subsequent attack by abrasive particles. Surface regions then fracture and loosened pieces are plowed off. Finally, many cracks, small voids, and pits form. This wear behavior is termed cracking and chipping brittle failure.

The wear resistance of the coating is related to its microstructure and primary phases. The mechanism that can explain increase in wear resistance by formation of nanophase particles in a residual amorphous matrix has been extensively discussed. The contribution can be divided into two kinds of effects, i.e., nanocrystalline particle effect and remaining amorphous phase effect [38]. As the former effect, the nanoscale α(Fe,Cr) particles have a perfect crystal structure leading to high strength, i.e., the α(Fe,Cr) particles are too small to contain dislocations. At the same time, shear sliding of the amorphous matrix can be suppressed by the homogeneous dispersion of the nanoscale α(Fe,Cr) particles. And nanoparticles can suppress cracks along the interface between the amorphous matrix and nanoscale particles. This is induced by the formation of a higher degree of dense-packed interface structure resulting from the lower interfacial energy at the amorphous/crystal interface as compared with the crystal/crystal interface energy [38]. Kim et al. [39] have pointed out that the nanocrystalline grains are too small to contain defects (such as dislocations, stacking faults) and their ultra-high strength would explain the greater resistance to deformation than the amorphous phase itself. In amorphous alloys, the deformation mechanism is inhomogeneous and involves shear on highly localized bands. Localized shear deformation can be effectively suppressed by interfaces (induced by nanocrystalline particles) or by a possible interaction between shear bands and a nanocrystalline phase [40]. Therefore, multiple interfaces should play an important role as the case with conventional precipitation-hardened nanoscale particles. It can be expected the nanocrystals act to dispersion strengthen the amorphous alloys increase the fracture stress, and decrease crack growth [41, 42]. As the latter effect, the remaining amorphous phase is insensitive to embrittlement caused by structural relaxation, leading to the large allowance to the precipitation of crystalline phases. The remaining amorphous phase can have a compressive residual stress field, multi-axis stress field, and localized deformation mode [38]. In addition, the elasticity of the amorphous/nanocrystalline coating is much higher than that of the substrate. The high ratio of hardness to elastic modulus (H/E) is indicative of good wear resistance [43]. Therefore the coating has excellent wear abrasive resistance.

Summary

FeCrBSiMnNbY metallic glass coatings were fabricated by wire-arc spray process. The microstructure of the coating consists of amorphous phase and α(Fe,Cr) nanocrystalline phase. The nanocrystalline grains are 30–60 nm in diameter and homogenously dispersed in the amorphous matrix.

The crystallization temperature of the amorphous phase is about 545 °C. The average adhesive strength value of the coating is 53.6 MPa. The nano-hardness and nano-elastic modulus of the coating are 15.74 and 216.97 GPa, respectively. The Vickers hardness of the coating reaches $Hv_{100} = 1031$ near the outside surface. The coating is fully dense with a porosity of 1.7%; little oxide is detected.

The relatively wear resistance of metallic glass coating is 7 and 2.3 times than that of substrate and 3Cr13 coating, respectively. The main failure mechanism of metallic glass coating is brittle failure and fracture. The Fe-based metallic glass coating has excellent wear resistance. The reasons are attributed to a uniform dispersion of nanocrystals in an amorphous matrix, and the high ratio of hardness to elastic modulus (H/E) of the coating.

Acknowledgement The authors are grateful for the support provided by Key Natural Science Foundation of China (50735006), National Key Laboratory for Remanufacturing (914OC85020508OC85), and Key Laboratory for Advanced Materials Processing Technology, Ministry of Education, People's Republic of China (200802).

References

1. Schuh CA, Hufnagel TC, Ramamurty U (2007) Acta Mater 55:4067
2. Inoue A, Shen BL, Chang CT (2004) Acta Mater 52:4093
3. Inoue A, Shinohara Y, Gook JS (1995) Mater Trans JIM 36:1427
4. Shen TD, Xchwarz RB (1999) Appl Phys Lett 75:49
5. Pawlik P, Davies HA, Gibbs MRJ (2003) Appl Phys Lett 83:2775
6. Wu X, Xu B, Hong Y (2002) Mater Lett 56:838
7. Kobayashi A, Yano S, Kimura H et al (2008) Surf Coat Technol 202:2513
8. Otsubo F, Kishitake K (2005) Mater Trans 46:80
9. Ni HS, Liu XH, Chang XC et al (2009) J Alloys Compd 467:163
10. Cherigui M, Fenineche NE, Ji G et al (2007) J Alloys Compd 427:281
11. Ajdelsztajn L, Jodoin B, Richer P et al (2006) J Therm Spray Technol 15(4):495
12. Sharma P, Zhang W, Amiya K, Kimura H, Inoue A (2005) J Nanosci Nanotechnol 5:416
13. Liu D, Gao W, Li Z et al (2007) Mater Lett 61:165
14. Thorpe ML (1993) Adv Mater Process 143(5):50

15. Newbery AP, Grant PS, Neiser RA (2005) Surf Coat Technol 195:91
16. Miyoshi K, Buckley DH (1984) Thin Solid Films 118:363
17. Masumoto T (1994) Mater Sci Eng A 179–180:8
18. Boswell PG (1979) J Mater Sci 14:1505. doi:10.1007/BF00549329
19. Fleury E, Lee SM, Ahn HS et al (2004) Mater Sci Eng A 276:375
20. Prakash B (2005) Wear 258:217
21. Klinger R, Feller HG (1983) Wear 86:287
22. Miyoshi K, Buckley DH (1983) ASLE Trans 27(4):295
23. Moreton R, Lancaster JK (1985) J Mater Sci Lett 4:133
24. Greer AL, Rutherford KL (2002) Int Mater Rev 47(2):87
25. Standard test method for adhesion or cohesion strength of thermal spray coatings C 633-01 (2001) Annual book of ASTM standards, ASTM
26. Wu Y, Lin P, Xie G et al (2006) Mater Sci Eng A 430:34
27. Ajdelsztajn L, Jodoin B, Richer P et al (2006) J Therm Spray Technol 15(4):495
28. Ma Q, Roth J, Gandy DW et al (2006) J Therm Spray Technol 15(4):670
29. Inoue A, Zhang T, Masumoto T (1989) Mater Trans JIM 30:965
30. De Boer FR, Boom R, Mattens WCM et al (1989) Cohesion in metals: transition metal alloys. North-Holland, Amsterdam, The Netherlands
31. Ponnambalam V, Poon SJ, Shiflet GJ (2004) J Mater Res 19:1320
32. Georgieva P, Thorpe R, Yanski A et al (2006) Adv Mater Process 8:68
33. Gedzevicius I, Valiulis AV (2006) J Mater Process Technol 175:206
34. Branagan DJ, Breitsameter M, Meacham BE et al (2005) J Therm Spray Technol 14(2):196
35. Branagan DJ, Kramer MJ, McCallum RW (1996) J Alloys Compd 244:27
36. Kobayashi A, Yano S, Kimura H et al (2008) Mater Sci Eng B 148:110
37. Pharr GM (1998) Mater Sci Eng A 253:151
38. Inoue A, Wang XM (2000) Acta Mater 48:1383
39. Kim YH, Higara K, Inoue A et al (1994) Mater Trans JIM 35:293
40. Gloriant T (2003) J Non-Cryst Solids 316:96
41. Leonhard A, Xing LQ, Heilmaier M et al (1998) Nanostruct Mater 10:805
42. Xing LQ, Eckert J, Schultz L (1999) Nanostruct Mater 12:503
43. Leyland A, Matthews A (2004) Surf Coat Technol 177–178:317